International Journal of Offshore and Polar Engineering (ISSN 1053-5381)

Vol. 30, No. 3, September 2020, pp. 257–265; https://doi.org/10.17736/ijope.2020.mm23

http://www.isope.org/publications

CFD Investigations of Wake Flow Interactions in a Wind Farm with 14 Wind Turbines

Xinze Duan, Jianhua Wang* and Decheng Wan*,†
Computational Marine Hydrodynamics Lab (CMHL), State Key Laboratory of Ocean Engineering, School of Naval Architecture, Ocean and Civil Engineering, Shanghai Jiao Tong University, Shanghai, China

Because the wake flow interaction phenomenon among wind turbines has a great influence on aerodynamic power output, wind speed deficit turbulence stress, and wake vortex structure, the wake interaction for the optimal arrangement of wind farm has recently attracted increasing attention. This paper presents a validation of aerodynamics for the two offset model wind turbines on the actuator line model and computational fluid dynamics (CFD) technique. The numerical results of the present simulations are compared with those produced by testing on Blind Test 3 and other simulation models. On the basis of the simulations results, the present study shows good agreement with the experimental results. Besides, considering the uniform inflow condition, a numerical method is harnessed to simulate the complex phenomenon of wake interaction in a wind farm containing 14 wind turbines. Large eddy simulations combined with an actuator line model are conducted in the in-house CFD code FOWT-UALM-SJTU solver, which is an extension based on OpenFOAM. The motivation for this work is to create a sound methodology for performing the simulation of large wind farms. To better understand the wake interaction phenomenon, the aerodynamic power coefficients and basic features of both the near and far wake, including the distribution characteristics of the mean wake velocity and vortex structures, are studied in detail.

INTRODUCTION

With the rapid development of wind energy technology, recent years have witnessed an increasing number of wind farms being built around the world to meet the demand for higher maximum wind power capacity (Jeon et al., 2013). Wind farms composed of large-capacity wind turbines are set to become the future trend of development of wind energy (Abderrazzaq and Hahn, 2006). However, wind turbines built in clusters will inevitably be affected by the wake of upstream and neighboring turbines, which leads to the decreased inflow wind velocity and increased turbulence intensity (Sanderse et al., 2011). Decreased total production of power and increased levels of fatigue loads are imposed on the turbines in the wind farm as a result of the phenomenon of wake interaction. Therefore, numerical simulations of a wind farm containing multiple wind turbines are carried out to study characteristics of aerodynamic power and the significant wake interference effect, which have very important scientific significance and practical reference value for wind farm layout optimization.

To study the complex phenomenon of wake interaction in wind farms, some scholars attempted to model the flow field in wind farms based on a simple single wake model. The wind wake model mainly describes the influence range of the wake and the wind speed at all positions in the wake area. The Park wake model, a kind of one-dimensional wake model, is extensively applied to model the flow field currently. The Park wake model was proposed by Katic et al. (1986) based on the Jensen model. It can analyze the wake interference in wind farms, and this theory is applied to the wind energy resource assessment software WAsP, which has a reliable accuracy. Inspired by the one-dimensional wake model, a wide spectrum of other wake models has been proposed, the dimensions of which are extended from one dimension to two or even three dimensions (Larsen et al., 1996; Schlez et al., 2001; Sanderse et al., 2011). Nevertheless, these wake models suffer a common disadvantage that the actual turbulent characteristics in the wake cannot be well captured. This flaw may lead to the underestimation of wake interference in the wind farms and the inability to accurately predict the aerodynamic loads because the significant effect of wake meandering is disregarded (Troldborg et al., 2011). Several researchers also attempted to use wind tunnel experiments to study the wake characteristics of a single wind turbine or the wake interaction in wind farms composed of small model wind turbines. Vermeer et al. (2003) researched the wake for a single turbine and wind farms with the uniform, steady, and parallel flow conditions using a wind tunnel experiment. Khosravi et al. (2015) carried out a wind tunnel experiment with single 1:300 scale model wind turbine, and the Froude number criterion is satisfied. The experimental results show that the wake effect of a wind turbine subjected to surge motion is much farther than a wind turbine without motion. Krogstad and Eriksen (2015) presented an experimental investigation of the aerodynamic load, wind velocity defect, and turbulent kinetic energy distribution in the wake of two model wind turbines with two different layouts, the results of which were compared with a wide range of methods. The drawback of the wind tunnel experiment is that a low Reynolds number and scale effects cannot be eliminated relative to the full-scale model. On the contrary, the advantage of CFD approach, which provides necessary information about wake characteristics, is that it can avoid the scale effect in the model experiment and handle the large Reynolds number problem well. From the work of Zahle et al. (2009) and Choi et al. (2013, 2014), numerical simulation of full three-dimensional (3-D) wind turbine models through resolving the blade geometry with its boundary layers is computation-

*ISOPE Member.
†Corresponding Author.
Received January 18, 2019; updated and further revised manuscript received by the editors June 25, 2019. The original version (prior to the final updated and revised manuscript) was presented at the Twenty-eighth International Ocean and Polar Engineering Conference (ISOPE-2018), Sapporo, Japan, June 10–15, 2018.
KEY WORDS: CFD, actuator line model, wake interaction, Blind Test 3, wind farms.

ally time consuming. As a result, it is hard to extend the full 3-D wind turbine model from a few wind turbines to large wind farms. A mixed method named the actuator line model (ALM) combined with a CFD technique, developed by Sørensen and Shen (2002), is an extensively used method to model the rotor as a force field. Troldborg et al. (2011) presented numerical simulations to analyze the phenomenon of a wake interaction between two wind turbines using the actuator line method and full unsteady Navier–Stokes computations coupled with EllipSys3D software (Michelsen, 1994; Sørensen, 1995). Churchfield, Lee, Moriarty, et al. (2012) had done a large eddy simulation of the Lillgrund wind plant, which contains 48 multi-megawatt turbines, and all the turbines were modeled using actuator line representation. Ai et al. (2017) presented numerical simulations to explore the effects of interturbine spacing changed from three to nine times the rotor diameter on aerodynamics for wind farms containing two NREL 5MW baseline wind turbines in tandem layout.

In this study, numerical validation of CFD combined with actuator line methods for modeling the rotors is conducted first. The numerical results of the present simulations are compared with those produced by testing on Blind Test 3 and other simulation models. Besides considering the uniform inflow condition, the complex phenomenon of wake interaction in a wind farm containing 14 wind turbines is simulated using a technique that combines an actuator line method with large eddy simulations (LES). The objective of the work is to create a sound methodology for performing the simulation of large wind farms and improve understanding of the wake interaction.

NUMERICAL METHODS

Actuator Line Model

The ALM was first developed by Sørensen and Shen (1999). The basic thought of this method is to replace the blades of the wind turbine with lines, the body forces of which are distributed radially. So the main advantage is that it is not required to build the actual blade model, as much fewer grid points are needed. Moreover, the lift force and drag force of each section can be calculated as

$$L = \frac{1}{2} C_l(\alpha) \rho U_{\text{rel}}^2 c dr \tag{1}$$

$$D = \frac{1}{2} C_d(\alpha) \rho U_{\text{rel}}^2 c dr \tag{2}$$

where C_l and C_d are the lift and drag coefficients, respectively. α is the attack angle, c is the chord length, and U_{rel} is the local velocity relative to the rotating blade of each section.

From Fig. 1, we can see that the local velocity relative to the rotating blade can be expressed as

$$U_{\text{rel}} = \sqrt{U_z^2 + (\omega r - U_\theta)^2} \tag{3}$$

Here, U_z and U_θ are the axial velocity and tangential velocity, respectively. The Ω is the rotational velocity of rotors. The body force f can be expressed as

$$f = (L, D) = \frac{1}{2} \rho U_{\text{rel}}^2 c dr \left(C_l \vec{e}_L + C_d \vec{e}_D \right) \tag{4}$$

The aerodynamic blade force cannot be directly applied to the flow field, and it needs to be distributed smoothly on the flow field volume in order to avoid singular behavior. In practice, a 3-D Gaussian function is used to smooth the force over the blade by taking the convolution of the force with a regularization kernel.

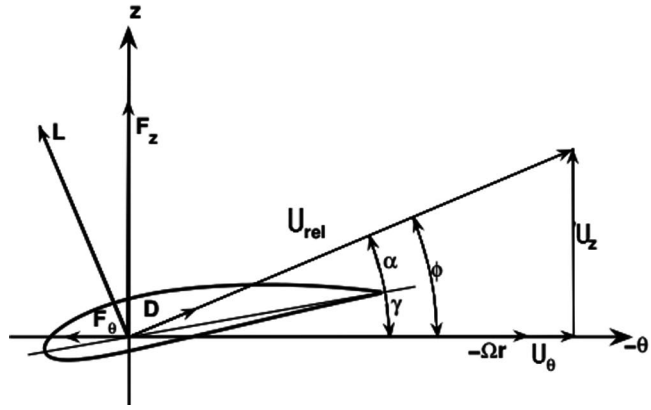

Fig. 1 Cross-sectional aero foil element (Sørensen and Shen, 2002)

$$f_\varepsilon = f \otimes \eta_\varepsilon \tag{5}$$

$$\eta_\varepsilon(d) = \frac{1}{\varepsilon^3 \pi^{3/2}} \exp\left[-\left(\frac{d}{\varepsilon} \right)^2 \right] \tag{6}$$

Here, d is the distance between cell-centered grid points and the actuator line point, and ε is a parameter that serves to control the width of the Gaussian and to adjust the concentration of the regularized loads.

Governing Equation

In recent years, the wake community has been more focused on the LES method because of its ability to handle unsteady and anisotropic turbulent flows dominated by large-scale structures and turbulent mixing (Sanderse et al., 2011; Cheng et al., 2019; Ning and Wan, 2019; Huang and Wan, 2020). In the LES model, a large-scale local averaged part $\overline{u}_i$ is directly calculated, whereas the eddies smaller than the grid part $\overline{u}_i'$ should be computed with a subgrid scale (SGS) model. The Navier–Stokes equations of incompressible flow, which are spatially filtered to arrive at the resolved scale, can be expressed as follows:

$$\frac{\partial \overline{u}_i}{\partial x_i} = 0 \tag{7}$$

$$\frac{\partial (\rho \overline{u}_i)}{\partial t} + \frac{\partial (\rho \overline{u_i u_j})}{\partial x_j} = -\frac{\partial \overline{p}}{\partial x_i} + \frac{\partial}{\partial x_j} \left[\mu \left(\frac{\partial \overline{u}_i}{\partial x_j} + \frac{\partial \overline{u}_j}{\partial x_i} \right) \right] + f_i^T \tag{8}$$

where f_i^T denotes the body force, which represents the loading on the blades exerted by the actuator line turbine model. The subgrid scale Reynolds stress τ_{ij} is defined as

$$\tau_{ij} = -\rho \left(\overline{u_i u_j} - \overline{u}_i \overline{u}_j \right) \tag{9}$$

The well-known Smagorinsky model is chosen as the subgrid stress model for turbulence closure:

$$\tau_{ij} - \frac{1}{3} \tau_{kk} \delta_{ij} = 2 \mu_t \overline{S}_{ij} \tag{10}$$

where μ_t is the eddy viscosity, $\overline{S}_{ij}$ is the strain rate of the large scale, and δ_{ij} is the Kronecker delta. The form of the subgrid scale eddy viscosity is

$$\mu_t = C_S^2 \rho \Delta^2 |\overline{S}| \tag{11}$$

The model constant C_s is set to 0.158. When applied to calculate the SGS heat flux, the resulting eddy-diffusivity model requires the specification of the lumped coefficient (Churchfield, Lee, Michalakes, and Moriarty, 2012). Note that $|\bar{S}| = \sqrt{2\bar{S}_{ij}\bar{S}_{ij}}$, and the stress rate is defined as

$$\bar{S}_{ij} = \frac{1}{2}\left(\frac{\partial \bar{u}_i}{\partial x_j} + \frac{\partial \bar{u}_j}{\partial x_i}\right) \tag{12}$$

and Δ denotes the filter length scale, $\Delta = (\Delta_x \Delta_y \Delta_z)^{1/3}$.

VALIDATION OF ALM

Experiment Description

The Blind Test 3 was organized by NORCOWE and NOWITECH in Bergen, Norway, on December 10 and 11, 2013. The wake development behind two model wind turbines that have been extensively tested in the large close-loop wind tunnel facility at NTNU. The two turbines were arranged offset so that downstream wind turbine can be affected by the partial impingement of the wake produced by the upstream turbine. Sketches of the layout are presented in Fig. 2, which shows two turbines mounted in the tunnel. The wind tunnel has a rectangle test section, whose dimensions at the inlet are $W = 2.72$ m and $H = 1.80$ m (where W means width and H means height). In addition, a large-scale biplanar grid was mounted at the entrance to the test section in order to imitate the atmospheric conditions. The reference velocity is set to $U_\infty = 10$ m/s. At this velocity, the turbulence intensity is $TI = 10\%$ at the inlet. More details about the Blind Test 3 can be found in Krogstad et al. (2015).

Furthermore, the two wind turbines have the same blade geometry but slightly different hub size, thus leading to a different rotor diameter. The diameters of upstream and downstream wind turbine are 0.944 m and 0.894 m, respectively. Table 1 presents the specification of the two wind turbines used in this study. In our setting, WT1 represents the upstream wind turbine, and WT2 is the downstream wind turbine.

Fig. 2 Wind tunnel

Items	WT1	WT2
Airfoil	S826	S826
Rotor diameter (m)	0.944	0.894
Nacelle diameter (m)	0.13	0.08
Height of tower (m)	0.817	0.817
Pitch angle	0	0
Tip speed ratio	6	4.75

Table 1 Parameters of two wind turbines

Items		Numerical value	Experiment	Relative error (%)
C_P	WT1	0.440	0.432	+1.852
	WT2	0.292	0.300	−2.667
C_T	WT1	0.801	0.771	+3.891
	WT2	0.570	0.547	+4.205

Table 2 Summary of numerical and experimental results for aerodynamic power and thrust coefficient

Results of Validation

The upstream wind turbine operates at a tip speed ratio 6, whereas the downstream wind turbine runs at a relatively lower tip speed ratio 4.75. The experimental value from the Blind Test 3 and the numerical value are summarized in Table 2.

Compared with experimental results, it can be concluded that the numerical simulations for two offset wind turbines modeled by the actuator line representation show good agreement with the aerodynamic load prediction in both power and thrust. Some discrepancies can be seen for both wind turbines, especially for the downstream one, but the highest error is not over 5%, which is tolerable in the engineering application. Meanwhile, Figs. 3 and 4 show the wake prediction including the mean wake velocity and mean turbulent stress at two positions ($X = 1D$ and $3D$, where

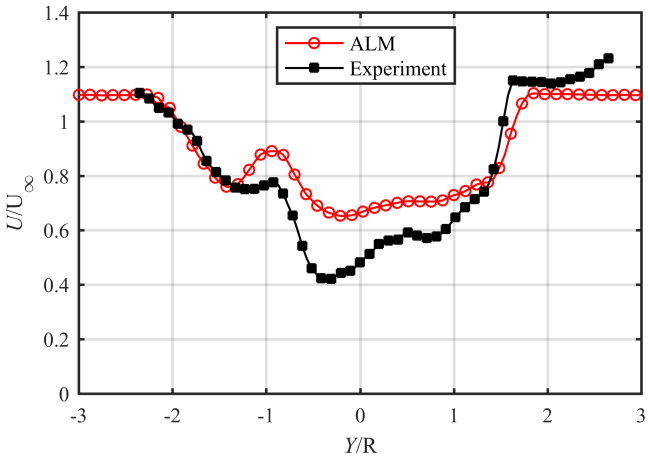

(a) Mean wake velocity

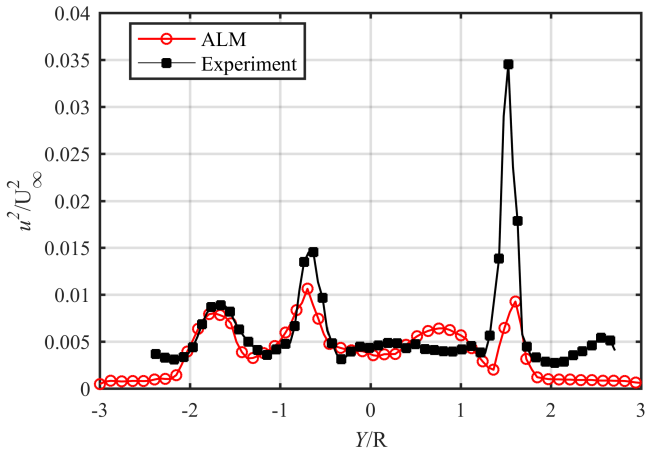

(b) Mean turbulent stress

Fig. 3 Wake prediction for mean wake velocity and mean turbulent stress at $X/D = 1$ behind the downstream wind turbine

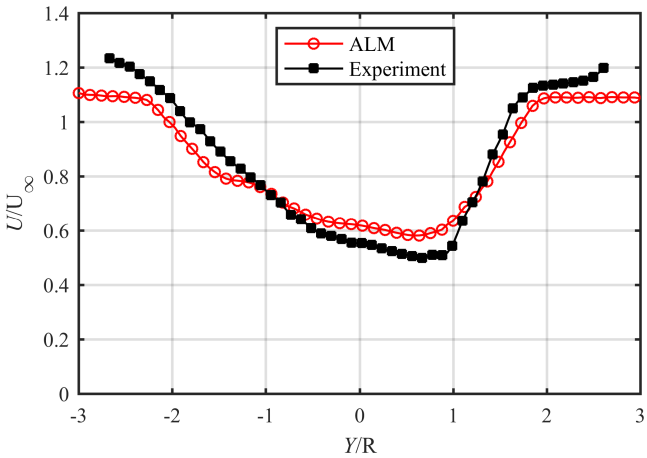

(a) Mean wake velocity

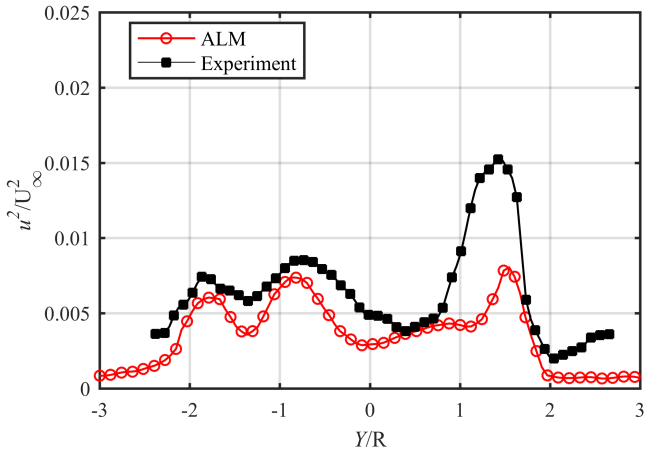

(b) Mean turbulent stress

Fig. 4 Wake prediction for mean wake velocity and mean turbulent stress at $X/D = 3$ behind the downstream wind turbine

D is the rotor diameter of the downstream turbine) behind the downstream wind turbine along the width direction. Note that the effects of the hub, nacelle, and tower are not included in the present simulation.

From the figures, the numerical value obtained by the ALM is marked with solid red circles. The mean wake velocity profile calculated by the simulation using the actuator line model is higher compared with the experimental results, marked in filled black squares. The current simulations do not take into account the effect of the nacelle and tower, leading to a lower prediction for the wind velocity deficit than that of an integrated wind turbine model. Besides, to a certain extent, the mean turbulent stress profile has good agreement with the experiment. Though the present study underestimates the turbulent stress magnitude especially in the peaks, the value of the turbulent stress magnitude is otherwise not much lower than that in the Blind Test 3.

According to the above discussion, in actuator line simulations, the boundary layers are not explicitly simulated, but their effect is taken into account via the lift and drag coefficients. Although the wake prediction has a certain gap between the numerical simulation and the experimental results, the actuator line model still can generate the distribution characteristics of the mean wake velocity and mean turbulent stress.

SIMULATION SETUP

The NREL 5MW baseline wind turbines were developed by the U.S. Department of Energy's National Renewable Energy Laboratory, and their blade airfoils consist of Cylinder, DU, and NACA 64 (Jonkman, 2010). In addition, the rotational direction of the rotor is clockwise, and the rotational phase of each wind turbine is synchronized. Table 3 gives the specifications of NREL 5MW baseline wind turbine used in this present study.

Rating	5 MW
Rotor orientation	Upwind
Number of blades	3
Rotor diameter, hub diameter	126 m, 3 m
Hub height	90 m
Cut-in, rating, cut-out	3 m/s, 11.4 m/s, 25 m/s
Cut-in, rating rotor speed	6.9 rpm, 12.1 rpm
Overhang, shaft tilt, precone angles	5 m, −5°, 2.5°

Table 3 Parameters of the NREL 5MW turbine

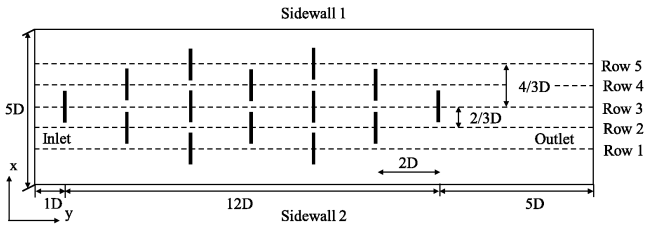

Fig. 5 The arrangement of the wind farm

Numerical simulations of a wind farm containing 14 wind turbines are conducted in this work. In the experiment setup, the height of hubs for each wind turbines and the longitudinal spacing between the two adjacent wind turbines are maintained at the same value equal to 90 m and $2D$, respectively. All distances are based on the rotor diameter D, equal to 126 m. There is a crosswind offset of 2/3 and 4/3 rotor diameters between the hub center of upstream turbine and the downstream turbines. The detailed arrangements are shown in Fig. 5. The width and height of the wind farm flow field are kept at $5D$ and $4D$, respectively. The distance $L1$ from the inlet to the upstream wind turbine and the distance $L2$ from the outlet to the latter downstream wind turbine are set to be $1D$ and $5D$, respectively. The downstream wind turbines are placed in the strong wake region of upstream wind turbines, which aims to reduce the total number of grid points and allows for observing the influence of wake interaction on the aerodynamics for the wind farm.

The grid extension regions for the whole numerical computation are differently imposed to fully resolve the strong gradients in the vicinity of the actuator lines and carefully observe significant meandering of the wake. The first part is the outer mesh, which is an initial mesh part for the whole flow field. From Fig. 6, it can be figured out that the range of the second part, which has one level refinement based on the initial mesh, is from a certain distance ahead of the first turbine to its end in the flow direction and from $-2D$ to $2D$ in width direction. The motivation of the mesh refinement is to capture the near wake characteristics for each wind turbine and study the phenomenon of wake interaction

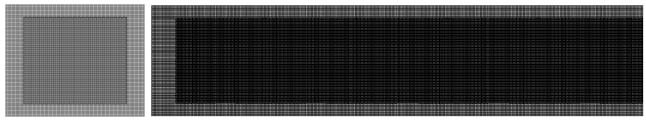

(a) Grid in cross section (b) Grid in lengthwise section

Fig. 6 The grid in lengthwise section and cross section

Inlet	11.4 m/s at the reference height
Outlet	Atmospheric pressure
Side	Symmetry
Top	Free-slip condition
Bottom	No-slip condition

Table 4 Boundary conditions

in detail. The minimum grid size is set to the moving distance of the blade tip for a 2.5° change in angle. The total mesh consists of about 14.5 million cells.

The uniform inflow model is used, ignoring the wind shear effect. Thus, the enforced conditions are set as follows: the free-stream flow velocity is equal to the rated speed 11.4 m/s, and the rotation speed of the blades of all wind turbines in the wind farm is the rated speed, 12.1 rpm. The detailed boundary conditions are listed in Table 4.

The duration of the whole computation is about 300 seconds to ensure the full development of the wake of all turbines in the wind farms, especially the last turbine that is seriously affected by the upstream turbine. The computational time-step size $\omega_b dt = 1$ degree per iteration is small enough to avoid numerical divergence, where the term ω_b is the rotation speed of the blades. Meanwhile, the Gaussian width parameter ε in Eq. 6 is utilized to adjust the concentration degree of the body force, because a smaller ε results in a more concentrated distribution of the volume force. Inspired by this observation, the value of ε is roughly the minimum at which the force is smoothed enough to avoid spurious oscillations in the resulting velocity field in a central spatial discretization scheme (Martínez et al., 2012). In this study, the parameter ε, kept equal to twice the local grid size around blades, is set to 5.

RESULTS AND DISCUSSION

In this study, the aerodynamics and complex phenomenon of the wake interaction among 14 wind turbines are explored based on the ALM combined with the CFD technique, including the characteristics of the instantaneous wake velocity profile and the wake velocity contour and the vortex structure.

Aerodynamic Loads

Because of the impulsive start-up problem of the rotor at the beginning of numerical simulations, both the upstream wind turbine and downstream turbines undergo a transient overshoot. To avoid the effect of the initial transient loads and ensure the full development of the wake, the average of aerodynamic loads of the 14 wind turbines was taken from 200 seconds to 300 seconds, shown in the statistical histograms in Figs. 7 and 8. Figure 7 represents the time average of aerodynamic power output, and Fig. 8 represents the time average of aerodynamic thrust output.

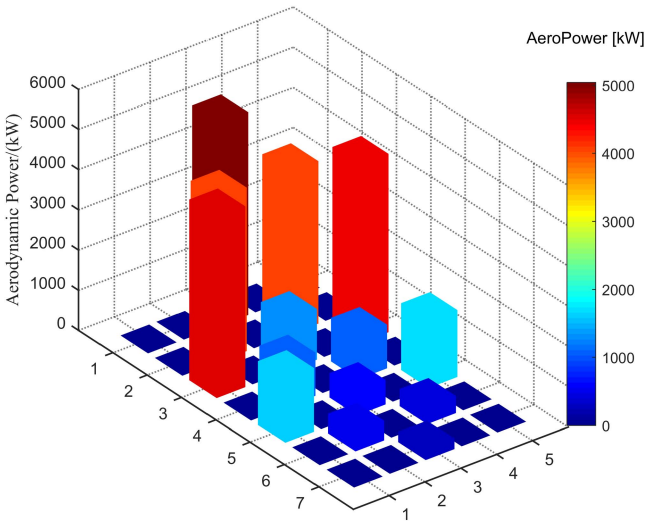

Fig. 7 Time average of aerodynamic power output

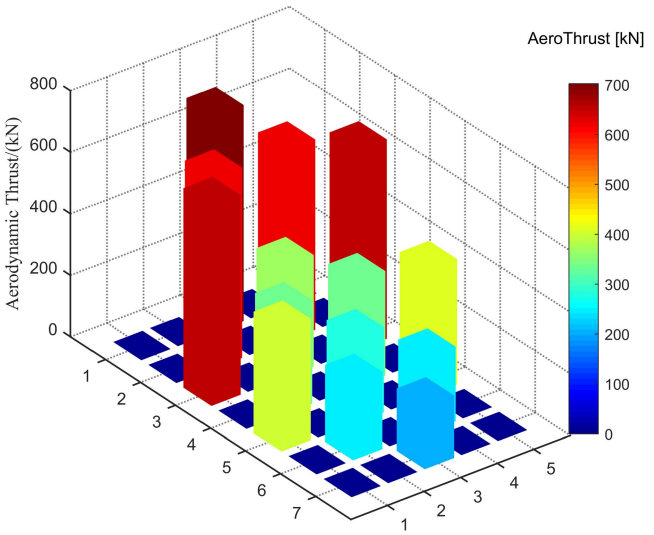

Fig. 8 Time average of aerodynamic thrust output

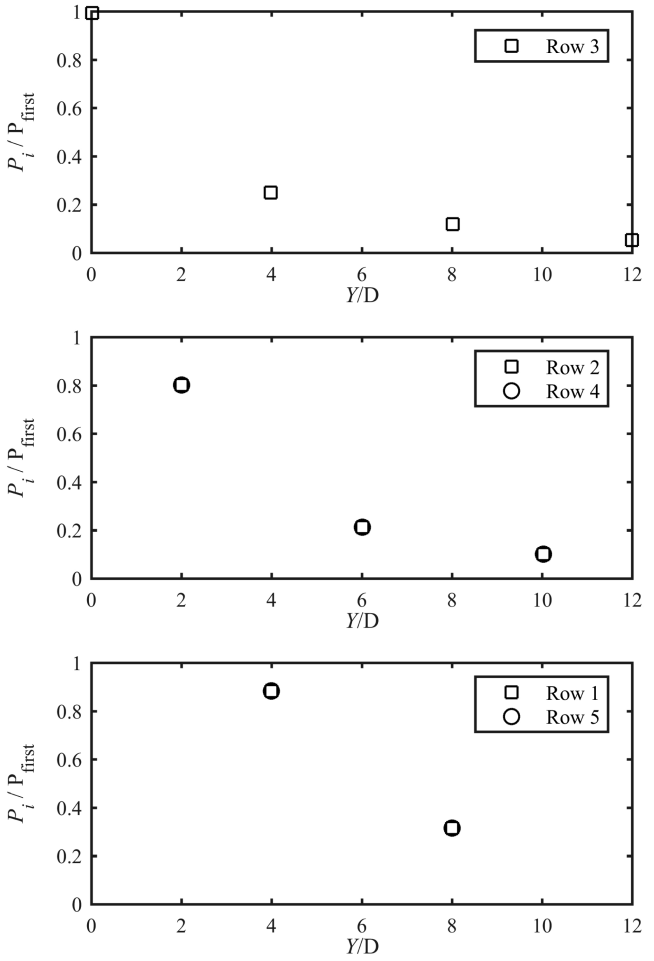

Fig. 9 Time-averaged aerodynamic power output produced by each turbine and normalized by the average power of the first turbine in row 3

From these figures, the power output of five wind turbines, which are located at the front position of rows 1 to 5, is close to the rated power. The turbine spacing along the direction of inflow is two rotor diameters, which is much closer than in real wind farms. Therefore, the obvious wind speed deficit compared with the inflow wind speed leads to a serious decrease in the aerodynamic power output and aerodynamic thrust of downstream wind turbines because of the wake effects. Compared with the significant reduction of the aerodynamic power, the reduction of aerodynamic thrust is much weaker. The reason for this phenomenon may be that although the inflow wind speed is decreased, the local angle of attack decreases at the same time, leading to the increased axial distribution of the local force of the blade. To recap, the aerodynamic power and thrust of downstream wind turbines are changed because of the strong interaction between the upstream and downstream wind turbines in the wind farms.

Figures 9 and 10 show the time-averaged aerodynamic loads produced by each turbine and normalized by the average power of the first turbine in row 3. The time-averaged power for the first turbines of these rows has decreased slightly; all the first turbines are affected by the partial impingement of the wake developed by the upstream turbine except the one in row 3.

Compared with the first turbine in each row, all second turbines, located in the wake region of upstream wind turbine, suffer a significant decrease in the aerodynamic power output by more than 70%. Because the upstream wind turbines absorb a large amount of energy from the air, the effective wind velocity

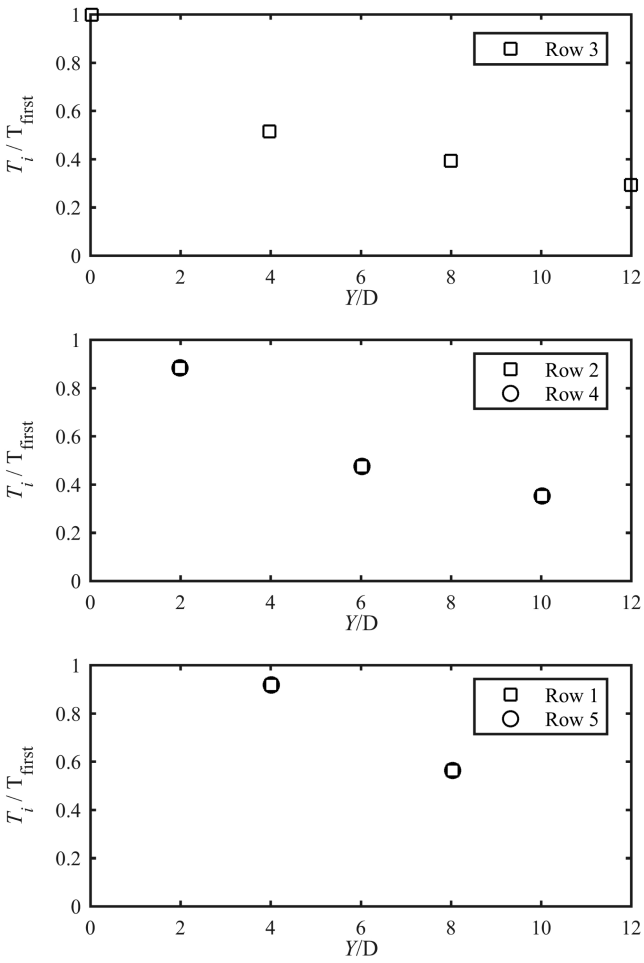

Fig. 10 Time-averaged aerodynamic thrust output produced by each turbine and normalized by the average thrust of the first turbine in row 3

is reduced in the downstream region compared with the inflow wind velocity. The longitudinal spacing between the two adjacent wind turbines is $2D$, so the wake velocity has not yet recovered in such a short distance. At this time, the wake flow passes through other wind turbines, and the wake is further developed. Meanwhile, the significant wake interaction effects and the mixed wake effects among the wind turbines aggravate the losses. Because of the lower inflow wind speed, the downstream wind turbines absorb less energy from the air, and thus, the wake effect is relatively weaker. Furthermore, with the continuous development of the wake flow, the wake effect gradually becomes increasingly weaker. As a result, the decrease of the aerodynamic power output of the wind turbine is no longer so obvious.

Wake Characteristics

Figure 11 shows the contour of instantaneous streamwise velocity in the horizontal plane (X-Y) through the center of the wind turbine rotor. Figures 12–14 show the contour of instantaneous streamwise velocity in the longitudinal plane (Y-Z) in each row. These figures are meaningful to understand the overall wake flow regions and find out which wind turbines mainly affect the wind speed. It can be clearly concluded that there are obvious changes of wind speed after the wind passes through the turbines.

From Figs. 11–14, it is easy to observe significant meandering of the wake, especially for the wake flows of downstream turbines. When the wake flow is disturbed by the wake of the other turbines, the turbulence characteristics of the wake are not very obvious, and the wake is in a relatively stable state. With the development of the wake, the wake flow is significantly instable

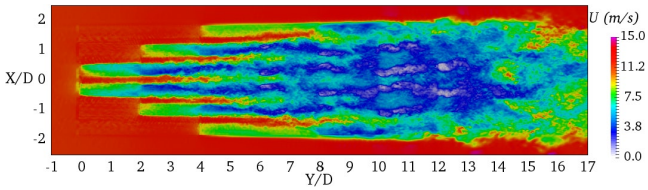

Fig. 11 The transient velocity contour at hub height in the X-Y plane

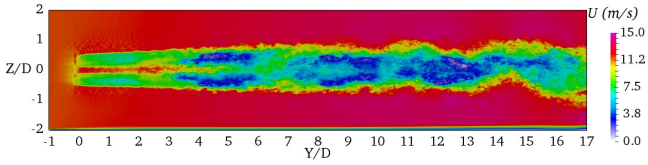

Fig. 12 The transient velocity contour in the Y-Z plane for row 3

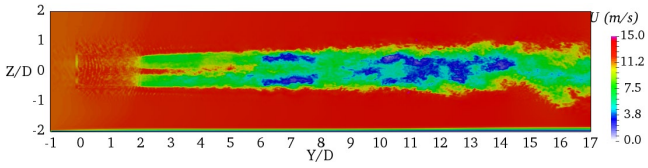

Fig. 13 The transient velocity contour in the Y-Z plane for row 2

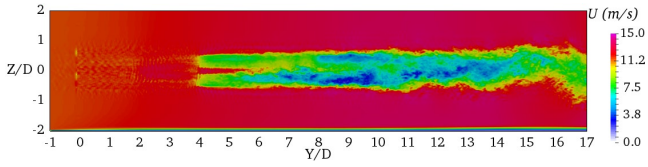

Fig. 14 The transient velocity contour in the Y-Z plane for row 1

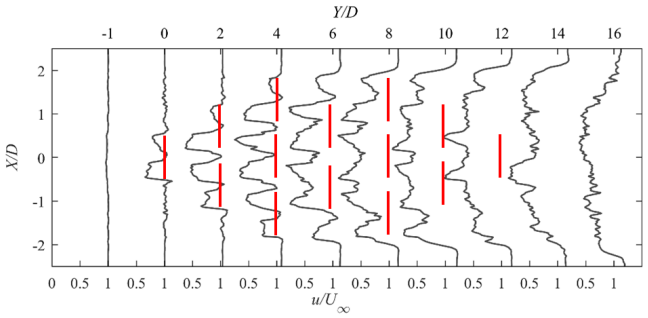

Fig. 15 The streamwise velocity at hub height in the X-Y plane

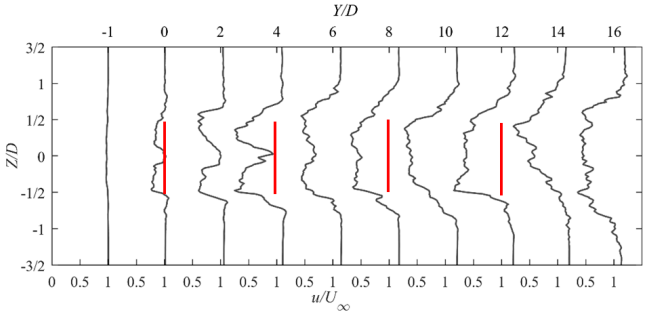

Fig. 16 The streamwise velocity in the Y-Z plane for row 3

along both the width and height, and the velocity is very complex and disordered. The extreme instability of wake velocity distribution reflects the significant turbulence characteristics of the wake. Because of the wake effect and the wake interaction among multiple wind turbines, the wake velocity is deficient and the turbulence intensity is enhanced. In addition, the meandering of these further downstream wakes is likely to be the cause of an increase in turbulent kinetic energy. Meanwhile, there is a higher speed region of flow near the center of the rotor. The reason for this phenomenon is that the effects of the hub, nacelle, and tower are not considered in the present simulation.

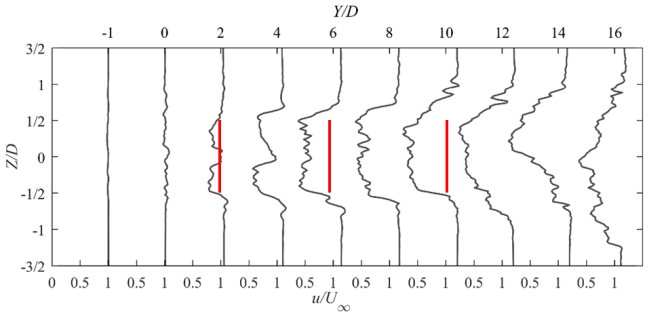

Fig. 17 The streamwise velocity in the Y-Z plane for row 2

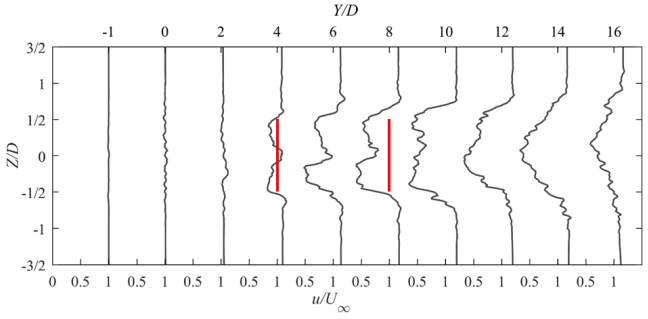

Fig. 18 The streamwise velocity in the Y-Z plane for row 1

Figure 15 shows the profile of the streamwise velocity at hub height in the X-Y plane. The corresponding profiles of the streamwise velocity in the Y-Z plane are shown in Figs. 16–18. The sharp decrease of the flow speed and the phenomenon of wake expansion can be clearly observed. The peaks pointing to the left represent the speed decrease, whereas values to the right indicate speed recovery. Because of the instantaneous streamwise velocity, there are many irregular fluctuations in the profiles of the wind speed, which are caused by the presence of significant meandering of the wakes. As the wake becomes increasingly turbulent, the horizontal asymmetry gradually diminishes. When the wind is aligned with the common axis of the turbines, the flow field downstream of the second turbine rapidly becomes fully turbulent at all inflow turbulence levels, mediated by the nonobvious effect of neglecting the hub, nacelle, and tower in the simulations.

Vortex Structure

Figure 19 shows the instantaneous vortex structure for the wind farms when the upstream vortex just encounters the downstream vortex, and Fig. 20 shows the instantaneous vortex structure in full development. It can be clearly seen that the tip vortex periodically sheds from each blade of the upstream wind turbine before the phenomenon of wake interaction happens. With the development of these vortices, the vortex generated by the upstream wind turbine is mixed with the vortices produced by downstream wind turbines. Consequently, the turbulent intensity is enhanced, and the vortex structure of wind field becomes very complicated. Meanwhile, the radius of the vortex structure becomes larger than the vortex that just sheds from the upstream wind turbine as a result of the wake expanding effects and the mixing. From the

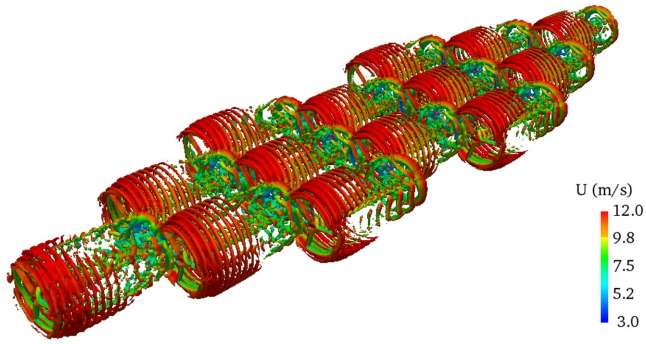

Fig. 19 The instantaneous vortex structure when the upstream vortex just encounters the downstream vortex

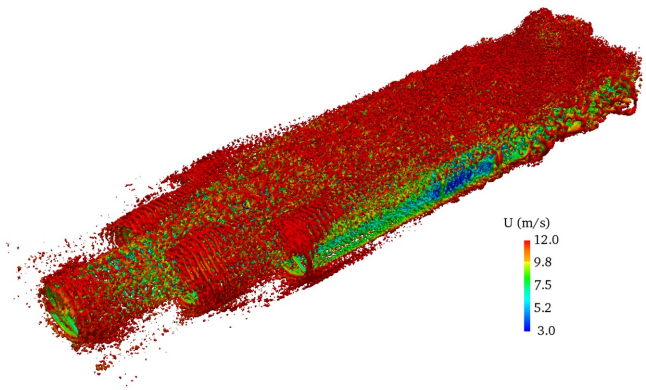

Fig. 20 The instantaneous vortex structure in full development of wake vortex

development of the vortex structure, it can be clearly seen that the strong and complex wake interaction phenomenon will lead to a wind speed deficit in the wind farm and severely disturb the aerodynamic power output of the downstream wind turbines.

CONCLUSIONS

In the present study, a numerical validation of CFD combined with actuator line methods for modeling the rotors is first conducted. The numerical results of the simulations are compared with their counterparts from the "Blind Test 3" and other simulation models. In this comparison, the present study shows good agreement with the experimental results, and the actuator line model also can clearly reproduce the distribution characteristics of the mean wake velocity and mean turbulent stress. Then the aerodynamics and complex phenomenon of wake interaction in a wind farm containing 14 wind turbines are analyzed successfully based on the actuator line model combined with the CFD technique, and the LES turbulence model is solved in the simulations conducted in OpenFOAM. From the results and discussion, it can be seen that when the longitudinal spacing between the two adjacent wind turbines is $2D$—which is much closer than in real wind farms—the wake velocity has not yet recovered. Therefore, the wake interaction between the upstream and downstream wind turbines in the studied wind farm has a strong effect on the aerodynamics of the wind turbines, leading especially to a significant reduction in the local wind speed and aerodynamic power output. Meanwhile, compared with the significant reduction of the aerodynamic power, the reduction of aerodynamic thrust is much weaker. Furthermore, the wake velocity is reduced and the turbulent intensity is enhanced as a result of the wake effect and the wake interaction among multiple wind turbines. Significant meandering of the wakes can be seen, many irregular fluctuations exist in the instantaneous profiles of the streamwise velocity, and the vortex structure of wind field becomes very complicated. In addition, the asymmetric interaction will result in significant unsteadiness in the aerodynamic power developed by the downstream turbines and more damaging fatigue loads on the blades of the turbines, which will reduce the lifetime of the wind turbines.

In future work, the wind shear effect and the impact of the turbulent inflow should be fully considered. Furthermore, the wind turbine tower and nacelle could be modelled with the actuator line method to consider the effect of the hub, nacelle, and tower in large wind farms, especially when simulating a full wind farm with tens or hundreds of turbines, where mesh generation for tower and nacelle would become very expensive.

ACKNOWLEDGEMENTS

This work is supported by the National Natural Science Foundation of China (Grants 51809169, 51879159), The National Key Research and Development Program of China (2019YFB1704200, 2019YFC0312400), Chang Jiang Scholars Program (T2014099), and Innovative Special Project of Numerical Tank of Ministry of Industry and Information Technology of China (2016-23/09), to which the authors are most grateful.

REFERENCES

Abderrazzaq, MA, and Hahn, B (2006). "Analysis of the Turbine Standstill for a Grid Connected Wind Farm (Case Study)," *Renewable Energy*, 31(1), 89–104. https://doi.org/10.1016/j.renene.2005.02.011.

Ai, Y, Wan, DC, and Hu, CH (2017). "Effects of Inter-turbines Spacing on Aerodynamics for Wind Farms Based on Actuator Line Model," *Proc 27th Int Ocean Polar Eng Conf*, San Francisco, CA, USA, ISOPE, 1, 386–394.

Cheng, P, Huang, Y, and Wan, DC (2019). "A Numerical Model for Fully Coupled Aero-hydrodynamic Analysis of Floating Offshore Wind Turbine," *Ocean Eng*, 173, 183–196. https://doi.org/10.1016/j.oceaneng.2018.12.021.

Choi, NJ, Nam, SH, Jeong, JH, and Kim, KC (2013). "Numerical Study on the Horizontal Axis Turbines Arrangement in a Wind Farm: Effect of Separation Distance on the Turbine Aerodynamic Power Output," *J Wind Eng Ind Aerodyn*, 117, 11–17. https://doi.org/10.1016/j.jweia.2013.04.005.

Choi, NJ, Nam, SH, Jeong, JH, and Kim, KC (2014). "CFD Study on Aerodynamic Power Output Changes with Inter-turbine Spacing Variation for a 6 MW Offshore Wind Farm," *J Energies*, 7(11), 7483–7498. https://doi.org/10.3390/en7117483.

Churchfield, MJ, Lee, S, Michalakes, J, and Moriarty, PJ (2012). "A Numerical Study of the Effects of Atmospheric and Wake Turbulence on Wind Turbine Dynamics," *J Turbul*, 13, N14. https://doi.org/10.1080/14685248.2012.668191.

Churchfield, MJ, Lee, S, Moriarty, PJ, et al. (2012). "A Large-eddy Simulation of Wind-plant Aerodynamics," *50th AIAA Aerosp Sci Meeting Exhibit*, Nashville, TN, USA, AIAA, 537. http://doi.org/10.2514/6.2012-537.

Huang, Y, and Wan, DC (2020). "Investigation of Interference Effects Between Wind Turbine and Spar-type Floating Platform Under Combined Wind-Wave Excitation," *Sustainability*, 12(1), 246. https://doi.org/10.3390/su12010246.

Jeon, SH, Cho, YU, Seo, MW, Cho, JR, and Jeong, WB (2013). "Dynamic Response of Floating Substructure of Spar-type Offshore Wind Turbine with Catenary Mooring Cables," *J Ocean Eng*, 72(7), 356–364. https://doi.org/10.1016/j.oceaneng.2013.07.017.

Jonkman, J (2010). *NWTC Design Codes* (*FAST*), https://nwtc.nrel.gov/FAST8.

Katic, I, Højstrup, J, and Jensen, NO (1986). "A Simple Model for Cluster Efficiency," in *Eur Wind Energy Assoc Conf Exhibit Proc*, W Palz, E Sesto (Eds), Rome, Italy, 1, 407–410.

Khosravi, M, Sarkar, P, and Hu, H (2015). "An Experimental Investigation on the Performance and the Wake Characteristics of a Wind Turbine Subjected to Surge Motion," *Proc 33rd Wind Energy Symp*, Kissimmee, FL, USA, AIAA, 1–18. https://doi.org/10.2514/6.2015-1207.

Krogstad, PÅ, and Ericksen, PE (2015). "'Blind Test' Calculations of the Performance and Wake Development for a Model Wind Turbine," *Renewable Energy*, 50, 325–333. https://doi.org/10.1016/j.renene.2012.06.044.

Krogstad, PÅ, Sætran, L, and Adaramola, MS (2015). "'Blind Test 3' Calculations of the Performance and Wake Development behind Two In-line and Offset Model Wind Turbines," *J Fluids Struct*, 52(1), 65–80. https://doi.org/10.1016/j.jfluidstructs.2014.10.002.

Larsen, GC, Højstrup, J, and Madsen, HA (1996). "Wind Fields in Wakes," in *Proc 1996 Eur Union Wind Energy Conf*, A Zervos, H Ehmann, P Helm (Eds), Göteborg, Sweden, HS Stephens & Associates, 764–768.

Martínez, LA, Leonardi, S, Churchfield, MJ, and Moriarty, PJ (2012). "A Comparison of Actuator Disc and Actuator Line Wind Turbine Models and Best Practices for Their Use," *50th AIAA Aerosp Sci Meeting Exhibit*, Nashville, TN, USA, AIAA, 900. https://doi.org/10.2514/6.2012-900.

Michelsen, JA (1994). *Block Structured Multigrid Solution of 2D and 3D Elliptic PDE's*, Technical Report AFM 94-06, Department of Fluid Mechanics, Technical University of Denmark, Kongens Lyngby, Denmark, 44 pp.

Ning, X, and Wan, DC (2019). "LES Study of Wake Meandering in Different Atmospheric Stabilities and Its Effects on Wind Turbine Aerodynamics," *Sustainability*, 11(24), 6939. https://doi.org/10.3390/su11246939.

Sanderse, B, Pijl, SP, and Koren, B (2011). "Review of Computational Fluid Dynamics for Wind Turbine Wake Aerodynamics," *J Wind Energy*, 14(7), 799–819. https://doi.org/10.1002/we.458.

Schlez, W, et al. (2001). "ENDOW: Improvement of Wake Models Within Offshore Wind Farms," *J Wind Eng*, 25(5), 281–287. https://doi.org/10.1260/030952401760177855.

Sørensen, JN, and Shen, WZ (1999). "Computation of Wind Turbine Wakes Using Combined Navier-Stokes/Actuator-line Methodology," *Proc 1999 Eur Wind Energy Conf Exhibit*, Nice, France, 156–159.

Sørensen, JN, and Shen, WZ (2002). "Numerical Modeling of Wind Turbine Wakes," *J Fluids Eng*, 124(2), 393–399. https://doi.org/10.1115/1.1471361.

Sørensen, NN (1995). *General Purpose Flow Solver Applied to Flow over Hills*, PhD thesis, Technical University of Denmark, Kongens Lyngby, Denmark, 156 pp.

Troldborg, N, et al. (2011). "Numerical Simulations of Wake Interaction Between Two Wind Turbines at Various Inflow Conditions," *Wind Energy*, 14(7), 859–876. https://doi.org/10.1002/we.433.

Vermeer, LJ, Sørensen, JN, and Crespo, A (2003). "Wind Turbine Wake Aerodynamics," *Prog Aerosp Sci*, 39(6), 467–510. https://doi.org/10.1016/S0376-0421(03)00078-2.

Zahle, F, Sørensen, NN, and Johansen, J (2009). "Wind Turbine Rotor—Tower Interaction Using an Incompressible Overset Grid Method," *Wind Energy*, 12(6), 594–619. https://doi.org/10.1002/we.327.